Vietnam Journal of Mechanics, VAST, Vol. 36, No 2 (2014), pp 109 - 118

A DIRECT EVIDENCE OF FATIGUE DAMAGE GROWTH INSIDE SILICON MEMS STRUCTURES OBTAINED WITH EBIC TECHNIQUE

Vu Le Huy[1,*], Shoji Kamiya[2]
[1] *Hanoi University of Science and Technology, Vietnam*
[2] *Nagoya Institute of Technology, Japan*
[*] E-mail: huy.vule@hust.edu.vn
Received October 16, 2013

Abstract. Electron beam induced current (EBIC) is a semiconductor analysis technique performed in a scanning electron microscope (SEM) or scanning transmission electron microscope (STEM). It is able to sense defects beneath the surface even invisible by SEM. This paper presents the results of a trial to observe the defect growth inside silicon MEMS structures under fatigue loading by applying EBIC technique. The tests were performed on two specimens fabricated from an n-type single crystal silicon wafer. While the test region of the specimens was repeatedly subjected to compressive stress, EBIC images were obtained to visualize damage evolution which presented by the growth of the dark region on EBIC images. It was proved that the damage is not due to the growth of oxidation layer on the surface of the specimens but due to the growth of intrinsic defects of silicon crystal. The results would be evidences to elucidate that the fatigue damages grow inside silicon MEMS structures but not in oxidation layer.

Keywords: EBIC, silicon, MEMS, defect, fatigue, dislocation.

1. INTRODUCTION

Microelectromechanical systems (MEMS) are devices with highly miniaturized mechanical components fabricated using batch processing techniques inspired by integrated circuit (IC) technologies, which have been among the fastest growing technologies, opening new frontiers of microtechnology [1, 2]. They have already been applied to various fields such as medical treatment and aerospace equipment where the reliability of MEMS structures is of serious concern. The mechanical reliability of MEMS has recently been attracting more and more interest.

Silicon is the most common structural material for MEMS. Since the end of the last century, many evidences have been found that they are susceptible to fatigue, which is the weakening of a material caused by repeatedly applied loads. Up to now, fatigue mechanism of micro-scale silicon structures is still under the debate. The most commonly accepted model of fatigue process has been the reaction layer model [3, 4], where the surface oxide layer is thickened with cyclic stress and subjected to corrosion cracking.

However, this theory could not explain for the case of low-cycle fatigue [5, 6], where the time was not enough for oxygen to diffuse into silicon. In contrast, however, it was also claimed that the thickening of a surface oxide layer due to cyclic stress was not observed until fatigue fracture on polysilicon devices with 3 nm thin native oxide [7] showing a counter evidence against the reaction layer model. Another mechanism was proposed that subcritical crack growth in silicon itself assisted through wedging of asperities on the crack surfaces [8, 9]. On the other hand, recent indirect evidences from the researches in Japan [10, 11] suggested another possibility of fatigue mechanism on the basis of dislocation mobility. For example, steps approximately 5 nm in height indicating dislocation slip lines were observed on the surface of 200 nm wide doubly supported beams made of single crystal silicon when bent with an atomic force microscope at 373 K [12]. Ductile behavior of nano-scale silicon at room temperature was also observed in other studies [13–15]. The fracture toughness of single crystal silicon films with 4 μm thickness was also reported to sharply increase above 70°C from 1.3 to 2.5 MPam$^{1/2}$ [16]. In other words, the increase of fracture toughness of single crystal silicon films at room temperature corresponds to the decrease of specimen thickness. This suggested that the increase in the dislocation mobility is related to the thickness reduction [11]. Dislocations emitted from the fracture surface created at room temperature in 1-μm-thick specimen were also directly observed with a transmission electron microscope [11]. The current understanding about the fatigue behaviors of silicon up to now is from the accumulation of experimental results and the observations on specimens after fatigue tests. Therefore, direct evidences to elucidate the fatigue mechanism of silicon structures in MEMS are necessary.

Electron beam induced current (EBIC) is known to be a semiconductor analysis technique performed in a scanning electron microscope (SEM) or scanning transmission electron microscope (STEM) [17]. It can be used to identify buried junctions or defects in semiconductors, or to examine minority carrier properties. It measures the current generated by the electron beam through a junction potential, which is able to sense defects beneath the surface even invisible by SEM. In this paper, EBIC technique is applied to see whether the defects eventually grow inside silicon under fatigue loading corresponding to the equivalent crack extension as modeled in our previous study [18]. Since it is expected that compressive stress accumulates the damage more efficiently [19], the observation in this study is performed with single crystalline silicon specimen tested with cyclic compressive stress. EBIC pictures should give direct evidences to elucidate fatigue mechanism of silicon MEMS structures.

2. EBIC TECHNIQUE

EBIC technique is based on the two schemes of setup as shown in Fig. 1 for the cases of plan-view and cross-section-identification. Plan view means that the p-n junction is perpendicular to the electron beam, whereas in cross-section-identification the p-n junction is parallel to the SEM beam. When an electron beam strikes a semiconductor sample, it will generate electron-hole pairs in an interaction volume. If they are near the p-n junction, they will diffuse to the junction. Electrons and holes will be drift to the n- type and p+ type, respectively. When the p+ and n- types are connected to a picoammeter or current

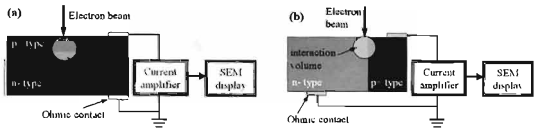

Fig. 1. Schemes of EBIC observation for (a) plan-view and (b) cross-section-identification

amplifier, they will produce an EBIC. This current can be used as the imaging signal for SEM or STEM. By connecting the EBIC signal scanned on observation region, EBIC image is obtained. For the case of plan-view, defects such as dislocations tend to strongly decrease the minority carrier in their vicinity, so the EBIC signal is strong in areas without the defects and weak in areas around the defects. Therefore, it should figure out the defects in silicon in terms of contrast change on its image.

3. SPECIMEN AND EXPERIMENTAL SETUP

3.1. Specimen

Fig. 2 shows the design of specimen used in EBIC observation experiment. The unit of dimensions is mm. The length and the thickness of the specimen are 18 mm and 0.38 mm, respectively. It was designed with a small test section in the upper part as a horizontal beam which is supported at both the ends by the two vertical arms connected to the base plate in the lower part. The length of the horizontal beam is 4 mm. Specimens were fabricated as schematically illustrated in Fig. 3 out of a n- type single crystal silicon wafer (thickness 380 μm, dopant Sb, conductivity 0.1 Ωcm) by applying a deep reactive ion etching (DRIE) process starting from the top surface of the wafer. The etched side surface has an inclination of 3 degrees, because of the characteristics of DRIE. Therefore,

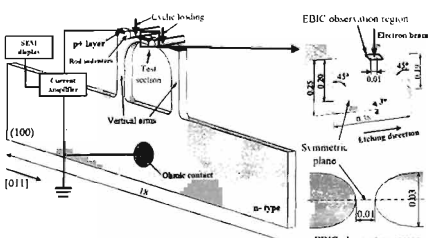

Fig. 2. Specimen used for EBIC observation

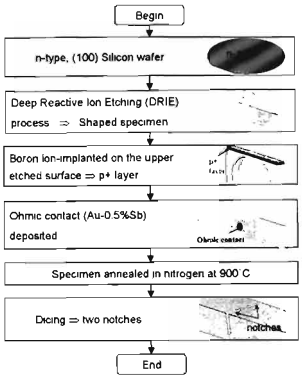

Fig. 3. Schematic illustration of fabrication process for the specimens

the heights of the cross section on the top and bottom surfaces of the wafer are 0.25 mm and 0.21 mm, respectively.

Boron was ion-implanted on the upper etched surface of the test section to compose a p+ layer, with the accelerating voltage of 5 kV and dosage of 1.0×10^{15} cm^{-2}. The junction underneath the p+ layer was utilized for the EBIC observation to explore the damage. For an ohmic contact to the n- type area, Au-0.5%Sb was deposited on the lower part of the specimen. The specimen was then annealed for 5 minutes in nitrogen at 900°C for the activation of dopants. Finally, two notches with 15 μm tip radius were created with a dicing saw, which were tilted by +45 and -45 degrees to the surface. The distance between the two notches was designed as 0.01 mm.

3.2. Experimental setup

Fig. 4 shows the experimental setup for EBIC observation of the specimen tested with cyclic loading. An environmental scanning electron microscope (ESEM) shown in Fig. 4(a) was used to perform EBIC observation. Specimen was kept by a state mounted on the holder inside the chamber of the ESEM as shown in Fig. 4(b). A piezo-positioner actuator (PI P-841.20, travel: 30 μm, resolution: 0.6 nm) was used to drive the setup as in Fig. 4(c). The applied load was measured by a load-cell LUR-A-100NSA1 manufactured by Kyowa Electronic Instruments Co., LTD. with a rated capacity 100 N. They were controlled by the equipments such as the computer, the function generator, etc., and monitored by the oscilloscope from outside of the chamber as shown in Fig. 4(a). The horizontal actuation given by the actuator was converted into the vertical stroke of loading rod indenters via

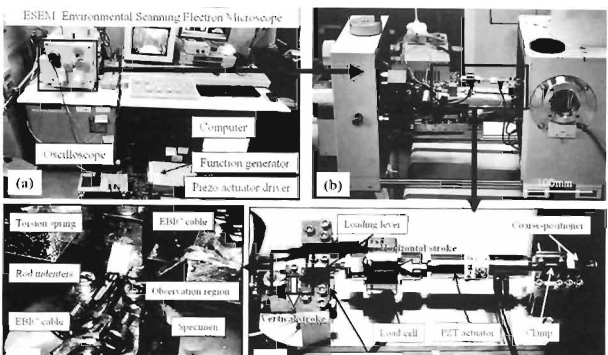

Fig. 4. Experimental setup for fatigue test in ESEM

an elastic torsion spring indicated in Fig. 4(c). These rod indenters pushed downward the upper surface of the test section at the two points indicated in Fig. 2 because of the inclination of the etched surface. The specimen was fixed to stand up vertically as shown in Fig. 4(d). By this way, the upper etched surface of the test section (indicated by EBIC observation region in Fig. 2) was facing to the electron beam while being subjected to a compressive stress. The EBIC cables shown in Fig. 4(d) are connected to the specimen and SEM display as illustrated in Fig. 2.

3.3. Evaluation of applied stress

The stress distribution on the EBIC observation region was analyzed by the finite element method (FEM) with ANSYS 14.0 software. In design, maximum compressive stress on the EBIC observation region was 75.6 MPa when the load applied to the specimen was 1 N. The distance between the two notches was expected to be 0.01 mm, but it was not able to be fabricated exactly. Therefore, FE analysis was performed individually for each specimen with the actual size of notches measured after creating the notches in order to obtain the exact value of the applied stress. Fig. 5 shows the stress distribution on the EBIC observation region of a specimen tested in this study. In this model, applied load was 20 N, and thus the maximum compressive stress is 1.57 GPa. The results obtained from FEM were used to calculate the maximum stress on the observation region when the load applied to specimen in the tests was known.

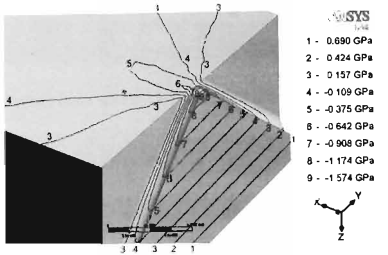

Fig. 5. Experimental setup for fatigue test in ESEM

4. RESULTS AND DISCUSSION

In this study, two specimens were tested by applying the cyclic loading with frequency of 50 Hz. The fatigue tests were occasionally interrupted to obtain EBIC images with an acceleration voltage of 30 kV as shown in Figs. 6 and 7. The properties and implemented conditions of these specimens are summarized in Tab. 1.

Table 1. Summarization of the specimens

Specimen number	#1	#2
Measured distance between the two notches (μm)	27	18
Gas pressure (Pa) inside ESEM chamber during fatigue test	560	40
Relative humidity (%)	20	4
Gas pressure (Pa) inside ESEM chamber when taking EBIC pictures	40	40
Applied maximum compressive stress (GPa)	0.89	0.82
Total number of cycles in fatigue test	2×10^5 cycles	5×10^5 cycles
Results of EBIC observation	Fig. 6(c)	Fig.7

For the first specimen (specimen #1), fatigue test was performed in the environment with gas pressure of 560 Pa which corresponds to 20% of relative humidity. Its SEM picture before the fatigue tests is shown in Fig. 6(a). Firstly, the maximum compressive stress applied to the EBIC observation region of the specimen was 0.62 GPa. EBIC pictures shown in Fig. 6(b) were taken during this test at gas pressure inside the ESEM chamber of 80 Pa. There was no noticeable change in the EBIC pictures from before the fatigue test (0 cycles) to after 5×10^5 cycles as shown in Fig. 6(b). This is consistent with the

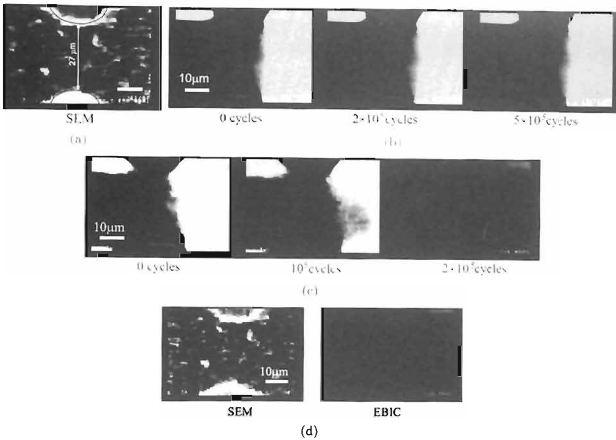

Fig. 6. Observation results of Specimen #1 with (a) SEM picture before the test, (b,c) EBIC pictures the during fatigue loading process when the applied compressive stress was (b) 0.62 GPa and (c) 0.89 GPa, and (d) after HF treatment

previous trial where the same stress level was applied to specimen but it was not able to see any clear change [20]. By increasing the maximum compressive stress to 0.89 GPa, the EBIC pictures were obtained as shown in Fig. 6(c). These EBIC pictures were taken at gas pressure inside the ESEM chamber of 40 Pa. The change in the EBIC pictures was clearly observed The dark region was seen to expand as the cycle number of applied load increases. After these fatigue tests, the specimen was etched by using 10%HF solution in 10 minutes, whose etch rate against thermal oxide is estimated to be 23 nm/min [21]. Therefore it should remove whole the silicon oxide layer, even if it would be so thick as 100 nm as presented in the other reports [4], locally exists at areas with stress concentration. If there would have been a locally grown silicon oxide layer on the surface to reduce EBIC, the image after HF treatment should have returned to the original image before fatigue loading. Fig. 6(d) shows the SEM and EBIC pictures of this specimen after etching. There was no marked difference between the EBIC images before and after HF treatment. Therefore, the changes in EBIC images were not due to the growth of surface oxide layer but growth of defects inside silicon.

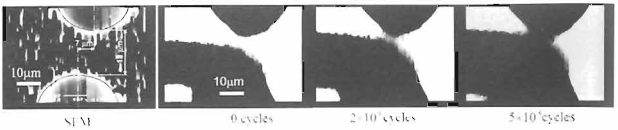

Fig. 7 Observation results of Specimen #2 when the applied compressive stress was 0.82 GPa

For the second specimen (specimen #2), fatigue test was performed in the environment with gas pressure of 40 Pa. The maximum compressive stress was 0.82 GPa. Its SEM and EBIC pictures were obtained as shown in Fig. 7. Gas pressure when taking those pictures was 40 Pa. The change in the EBIC pictures was also observed as the dark region gradually widening with the increment of number of cycles. With gas pressure of 40 Pa in this fatigue test corresponded to 4% of relative humidity, the effect of oxidation is negligible, and therefore HF treatment is not necessary for this specimen. On the other hand, the results show that the velocity of the dark region growth on the specimen #2 was slower than that of the specimen #1 due to the lower level of applied stress. It means that the expansion of the dark region presents an accumulation process of recombination defects generated in crystal during fatigue loading, which reduced the EBIC signal.

5. CONCLUSION

In this study, EBIC technique was applied successfully to observe the growth of defects inside silicon MEMS structures. The changes of local contrast were successfully observed at the notch tip of the specimens, which remained the same through the hydrofluoric acid treatment after the experiment. The damage, which caused the local contrast changes, was not the thickened surface oxide layer but the evolution of intrinsic defects being likely dislocations inside the crystal of silicon. These are the first direct evidences of fatigue mechanism in silicon. However, the resolution of the obtained EBIC pictures in this study is not high enough to estimate the structure of damage. To further elucidate the fatigue mechanism in silicon MEMS structures, experiment with EBIC observation is necessary to be improved to obtain the pictures at atomistic scale by using EBIC technique with high resolution SEM or STEM.

REFERENCES

[1] H. Fujita. Microactuators and micromachines. In *Proceedings of the IEEE*, Vol. 86. IEEE, (1998), pp. 1721–1732.

[2] M. J. Madou. *Fundamentals of microfabrication: The science of miniaturization*. CRC press, (2002).

[3] C. L. Muhlstein, S. B. Brown, and R. O. Ritchie. High-cycle fatigue of single-crystal silicon thin films. *Journal of Microelectromechanical Systems*, **10**. (4), (2001), pp. 593–600.

[4] C. Muhlstein, E. Stach, and R. Ritchie. A reaction-layer mechanism for the delayed failure of micron-scale polycrystalline silicon structural films subjected to high-cycle fatigue loading. *Acta Materialia*, **50**, (14), (2002), pp. 3579–3595.

[5] E. Baumert, P.-O. Theillet, and O. Pierron. Investigation of the low-cycle fatigue mechanism for micron-scale monocrystalline silicon films. *Acta Materialia*, **58**, (8), (2010), pp. 2854–2863.

[6] P.-O. Theillet and O. Pierron. Fatigue rates of monocrystalline silicon thin films in harsh environments: Influence of stress amplitude, relative humidity, and temperature. *Applied Physics Letters*, **94**, (18), (2009), pp. 181915–181915.

[7] H. Kahn, A. Avishai, R. Ballarini, and A. Heuer. Surface oxide effects on failure of polysilicon MEMS after cyclic and monotonic loading. *Scripta Materialia*, **59**, (9), (2008), pp. 912–915.

[8] H. Kahn, R. Ballarini, J. Bellante, and A. Heuer. Fatigue failure in polysilicon not due to simple stress corrosion cracking. *Science*, **298**, (5596), (2002), pp. 1215–1218.

[9] H. Kahn, R. Ballarini, and A. Heuer. Dynamic fatigue of silicon. *Current Opinion in Solid State and Materials Science*, **8**, (1), (2004), pp. 71–76.

[10] N. Kato, A. Nishikawa, and H. Saka. Dislocations in Si generated by fatigue at room temperature. *Materials Science in Semiconductor Processing*, **4**, (1), (2001), pp. 113–115.

[11] S. Nakao, T. Ando, S. Arai, N. Saito, and K. Sato. Variation in dislocation pattern observed in SCS films fractured by tensile test: Effects of film thickness and testing temperature. In *MRS Proceedings*, Vol. 1052. Cambridge Univ Press, (2007).

[12] T. Namazu, Y. Isono, and T. Tanaka. Plastic deformation of nanometric single crystal silicon wire in AFM bending test at intermediate temperatures. *Journal of Microelectromechanical Systems*, **11**, (2), (2002), pp. 125–135.

[13] X. Han, K. Zheng, Y. Zhang, X. Zhang, Z. Zhang, and Z. L. Wang. Low-temperature in situ large-strain plasticity of silicon nanowires. *Advanced Materials*, **19**, (16), (2007), pp. 2112–2118.

[14] F. Östlund, K. Rzepiejewska-Malyska, K. Leifer, L. M. Hale, Y. Tang, R. Ballarini, W. W. Gerberich, and J. Michler. Brittle-to-ductile transition in uniaxial compression of silicon pillars at room temperature. *Advanced Functional Materials*, **19**, (15), (2009), pp. 2439–2444.

[15] J. Nowak, A. Beaber, O. Ugurlu, S. Girshick, and W. Gerberich. Small size strength dependence on dislocation nucleation. *Scripta Materialia*, **62**, (11), (2010), pp. 819–822.

[16] S. Nakao, T. Ando, M. Shikida, and K. Sato. Effect of temperature on fracture toughness in a single-crystal-silicon film and transition in its fracture mode. *Journal of Micromechanics and Microengineering*, **18**, (1), (2008), p. 015026.

[17] C. Parish, D. Batchelor, C. Progl, and P. Russell. Tutorial: Electron beam-induced current in the scanning electron microscope. *Microscopy and Analysis*, **21**, (2007), pp. 11–13.

[18] V. L. Huy, J. Gaspar, O. Paul, and S. Kamiya. Statistical characterization of fatigue lifetime of polysilicon thin films. *Sensors and Actuators A: Physical*, **179**, (2012), pp. 251–262.

[19] K. Shima, S. Izumi, and S. Sakai. Reaction pathway analysis for dislocation nucleation from a sharp corner in silicon: Glide set versus shuffle set. *Journal of Applied Physics*, **108**, (6), (2010), DOI: 10.1063/1.3486465.

[20] S. Kamiya, R. Hirai, H. Izumi, N. Umehara, and T. Tokoroyama. Direct observation of damage accumulation process inside silicon under mechanical fatigue loading. In *Proceedings of the 17th International Conference on Solid-State Sensors, Actuators and Microsystems, Transducers & Eurosensors XXVII*, (2013), pp. 784–787.

[21] K. R. Williams, K. Gupta, and M. Wasilik. Etch rates for micromachining processing-part II. *Journal of Microelectromechanical Systems*, **12**, (6), (2003), pp. 761–778.